Theor Chim Acta (1990) 77: 369–382

Theoretica Chimica Acta

Chemical species conversion in condensed systems or at interfaces: quantum and classical regime of anharmonic Franck–Condon transitions

H. Schultz, C. Engler, and W. Lorenz
Sektion Chemie, Universität Leipzig, DDR-7010 Leipzig, German Democratic Republic

Received February 18 1990; received in revised form May 2, 1990/Accepted May 17, 1990

Summary. The relation of quantum to classical regime of Franck–Condon transitions is investigated, focussing on transitions in diabatic, anharmonic 1D potentials of a reactive subsystem which allow for chemical bond formation and partial charge transfer. A survey of numerical results is given for the range of both regimes under different system characteristics, including the diabatic barrier height of the reactive subsystem, the transfer distance (barrier breadth), and the reduced mass (1 to ∞) of the reactive mode. Energy distribution of transition components and of state-resolved statistical lifetimes are briefly discussed.

Key words: Quantum and classical regime – Franck–Condon transitions – Diabatic anharmonic potentials – Energy distribution of transition components

1. Introduction

Recent developments towards an approach of chemical charge transfer processes in condensed systems or at interfaces in terms of Franck–Condon transitions on diabatic (or quasiadiabatic) local potential surfaces, have strengthened the demand for investigating strong anharmonic potentials and heavy-particle transfer over larger distances. In a preceding paper [1] we have taken into consideration heavy-atom or atom-group transfer over distances up to 240 pm, in order to get certain hints about local potential surface shapes compatible with kinetic data for electrochemical dark and photoprocesses on semiconductors. In this context, both the quantum and classical regimes of Franck–Condon transitions have briefly been taken into account.

In pursuing this line of research, it has proved desirable to explore in greater detail the relationship of quantum to classical regime of transition probabilities in diabatic anharmonic potentials. Starting with the known quantum-statistical expression of the canonical transition probability of species conversion in a reactive subsystem, S, interacting with a classical medium, M (see below Eq. (1)), one gets in the classical limit for the total system $(S + M)$ an expression (see below Eq. (4)) which corresponds to reduced mass $\mu \to \infty$ of the reactive mode (in the calculations of this paper we limit ourselves to a 1D reactive subsystem).

An important characteristic of the processes under discussion is the distribution of transition components over initial-state vibration energies [2–4]. This distribution is accessible to calculation, in the quantum regime up to reduced mass of about 100 g mol^{-1}. It degenerates in the classical limit into a continuous distribution which retains a finite width, due to multidimensionality of the total system ($S + M$). A related characteristic is the distribution of statistical lifetimes of initial states in a canonical ensemble up to reactive transition into final states. Both features are of interest with regard to the short-time limits of the canonical, or sudden, approximation, which are coarsely attained in the time-scales of equilibration of the reactive mode and the medium.

In this paper, the following specific topics will be addressed and relevant results proved:

(a) The smooth transition from the quantum to the classical regime.

(b) Trends in the transition probability quotient for finite reduced mass (quantum regime) to infinite reduced mass (classical regime), with variation of the diabatic barrier height and the transfer distance (barrier breadth) of the reactive subsystem.

(c) Dependence of transition probabilities in the classical limit at fixed barrier, upon transfer distance; comparison of Franck–Condon models with the adiabatic activation picture.

(d) Influence of transfer distance upon tunneling in the quantum regime (small reduced mass).

(e) Relation of the diabatic barrier height of the reactive subsystem to activation parameters of the total system.

(f) Transition probability shift over medium reorganization energy and generalization to anharmonic subsystems coupled to a harmonic medium.

(g) Discussion of transition component and statistical lifetime distributions.

(h) Discussion of dynamical equilibration effects on transition component distribution and total transition probability.

2. Basic relations

We shall first briefly summarize the basic relations used in the subsequent calculations. The quantum-statistical expression of the canonical transition probability of a chemical conversion process in a reactive subsystem, S, interacting with a classical harmonic medium (see [1–4] and references therein), is

$$\langle P_{a\to b}\rangle^{qu} \equiv \sum_v \sum_w P_{av\to bw} = (\pi/\hbar^2 E_M kT)^{1/2} (Z_a^{qu})^{-1} \cdot \sum_v \sum_w f(v) \cdot g(w, v), \quad (1)$$

where $f(v) = \exp \beta E_{aSv}$, $\beta = -1/kT$

$$g(w, v) = |T^S_{bw,av}|^2 \cdot \exp \beta[E_{bSw} - E_{aSv} + E_M + \Delta E]^2/4E_M.$$

$P_{av\to bw}$ are transition components from vibration state v in the initial potential a to state w in the final potential b of the reactive subsystem S. E_{aSv} and E_{bSw} are the corresponding vibration energies (dependent on reduced mass; Eq. (1) is

moreover valid with many-dimensional, non-separable potentials). $Z_a^{qu} = \sum_v f(v)$ is the quantum partition function of the initial states. Transition matrix elements of the subsystem S are usually subjected to the Condon approximation, $T^S_{bw,av} \simeq V \cdot \langle bw|av\rangle$, with V the electronic matrix element and $\langle bw|av\rangle$ the Franck–Condon overlap. ΔE is the total energy minima difference of states a and b, and E_M the classical reorganization energy of a harmonic medium. Some calculational annotations are made in the appendix.

The distribution over E_{av} of transition components from initial state av to any final states b is given by

$$P_{av\to b} \equiv \sum_w P_{av\to bw} = (\pi/\hbar^2 E_M kT)^{1/2} \cdot f(v) \cdot (Z_a^{qu})^{-1} \cdot \sum_w g(w, v). \tag{2}$$

Division of $P_{av\to b}$ by the Boltzmann factor yields the reciprocal statistical lifetime of initial states in a canonical ensemble up to reactive transition:

$$1/\tau_{av} = P_{av\to b} \cdot [f(v)/Z_a^{qu}]^{-1}. \tag{3}$$

In the classical limit of the total system, the transition probability is in Condon approximation,

$$\langle P_{a\to b}\rangle^{cl} = (\pi/\hbar^2 E_M kT)^{1/2} \cdot V^2 \cdot (Z_a^{cl})^{-1} \cdot \int_{-\infty}^{+\infty} dR \cdot \exp \beta e(R), \tag{4}$$

where

$$e(R) = E_a(R) + [E_b(R) - E_a(R) + E_M + \Delta E]^2/4E_M.$$

Equation (4) is valid in arbitrary initial and final potentials $E_a(R)$, $E_b(R)$ of the reactive subsystem (requiring separability of many-dimensional potentials, contrary to Eq. (1)). Z_a^{cl} represents a classical limit of the partition function of initial states, likewise expressed as integral over R. Both Z_a^{cl} and the last integral in (4) have the dimension of R which is thus cancelled from Eq. (4).

Diabatic 1D model potentials of the initial and final states are chosen as Morse potentials

$$E(R) = D[1 - \exp(-a(R - R_0))]^2, \tag{5}$$

where R_0 labels the potential minimum, $D = k/2a^2$ is a bond dissociation energy, and k the harmonic force constant. With anharmonicity parameter $a \to 0$ and $D \to \infty$, Eq. (5) turns into a harmonic potential.

A classical analogue $P(E_a)^{cl}$ of the transition component distribution over initial energies E_a can be based on the quantal-classical correspondence

$$\langle P\rangle^{qu} = \sum_v P_{av\to b}, \qquad \langle P\rangle^{cl} = \int dE_a \cdot P(E_a)^{cl}. \tag{6}$$

Equations (6) and (4) are obeyed with

$$P(E_a)^{cl} = (\partial E_a/\partial R)^{-1} \cdot (\pi/\hbar^2 E_M kT)^{1/2} \cdot V^2 \cdot (Z_a^{cl})^{-1} \cdot \exp \beta e(R), \tag{7}$$

where $\partial E_a/\partial R$ is taken from (5); Eq. (7) includes separate contributions of both sides of the Morse curve, $R > R_0$ and $R < R_0$. Equal dimension of quantal and classical transition component distribution could be achieved by dividing $P_{av\to b}$ through $\hbar\omega_{av}$; in Figs. 5 and 6 below we renounce this transformation since it leaves the distribution shape unchanged.

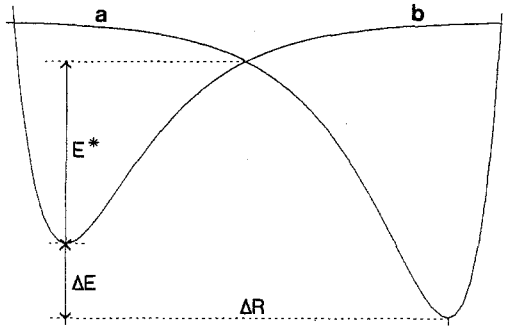

Fig. 1. Diabatic 1D potentials of initial and final state of the reactive subsystem. Comment see text

3. Calculations

A typical diabatic potential representation of initial and final states a and b of a reactive 1D subsystem is sketched in Fig. 1. It shows three essential parameters of the forward process $a \rightarrow b$ to be considered in the following: the transfer distance, or potential minima distance ΔR; the total energy zero point difference ΔE (including the medium energy difference of states a and b); and the diabatic barrier height E^* of the subsystem S (depending on initial and final potential shapes and on ΔE; the latter dependence includes a minor medium effect).

3.1. Smooth transition from quantum to classical regime

Some data which establish a smooth transition from the quantum to the classical regime of transition probabilities, $\langle P \rangle$, are given in Tables 1 and 2. Data with reduced mass $\mu = 1$ to 100 g mol^{-1} were calculated from Eq. (1); the data with $\mu \rightarrow \infty$ correspond to the classical limit and are obtained from Eq. (4). As a general feature of these examples, and also of a great number of further calculations, one recognizes a monotonous decrease of $\langle P \rangle$ with increasing reduced mass μ, or decreasing vibration quantum $\hbar\omega$, up to the classical limit (possible exceptions concern very low temperature and very large force constant and are mostly irrelevant). The temperature dependence of $\langle P \rangle$ included in Tables 1 and 2 will be commented on below in Sects. 3.5 and 3.6.

With increasing reduced mass, a greater number of transition components $P_{av \rightarrow bw}$ contribute significantly to the total transition probability. Computational techniques for anharmonic Franck–Condon overlap following [2–4] are addressed in the appendix. A typical limitation in the calculation of quantal transition probabilities $\langle P \rangle^{qu}$ can occur at large ΔR, when E^* lies near the Morse dissociation limit D of at least one of the two intersecting potentials, and there are still large transition components near D. Calculation of $\langle P \rangle^{qu}$ then possibly becomes unsafe. Relevant conclusions are drawn in the subsequent section.

Table 1. Transition probabilities $\langle P \rangle$ in the quantum regime (reduced mass 1 to 30) and classical regime (reduced mass ∞)

$k_a = k_b = 20\ \mathrm{N\ m^{-1}}$, $D_a = D_b = 4\ \mathrm{eV}$; $E_M = 2\ \mathrm{eV}$; $V^2 = 0.1\ \mathrm{eV^2}$; $\Delta R = 80\ \mathrm{pm}$

T/K	μ/g mol^{-1}	$\lg\langle P_{a\to b}/\mathrm{s^{-1}}\rangle$		
	for ΔE/eV =	−0.2	0	+0.2
	E^*/eV =	0.011	0.085	0.211
100	1	−7.1	−11.9	−17.1
	10	−8.8	−13.6	−18.9
	30	−9.1	−13.9	−19.1
	∞	−9.3	−14.1	−19.3
300	1	7.1	5.5	3.75
	∞	6.9	5.3	3.55

$k_a = k_b = 600\ \mathrm{N\ m^{-1}}$, $D_a = D_b = 4\ \mathrm{eV}$; $E_M = 0.5\ \mathrm{eV}$; $V^2 = 0.1\ \mathrm{eV^2}$; $\Delta R = 80\ \mathrm{pm}$

T/K	μ/g mol^{-1}	$\lg\langle P_{a\to b}/\mathrm{s^{-1}}\rangle$		
	for ΔE/eV =	−0.5	0	+0.5
	E^*/eV =	1.09	1.34	1.59
100	1	6.6	0.4	−18.5
	10	−11.8	−21.3	−37
	30	−28	−40	−53
	∞	−46	−59	−71
300	1	7.2	4.3	−1.2
	10	−2.8	−7.0	−11.2
	30	−4.3	−8.6	−12.7
	∞	−5.1	−9.7	−13.5

3.2. Trends in the transition probability quotient $\langle P \rangle^{qu}/\langle P \rangle^{cl}$ with variation of E^* and ΔR

Figure 2 shows on a logarithmic scale the transition probability quotient $\langle P \rangle^{qu}/\langle P \rangle^{cl}$ referring to the extreme cases of reduced mass $\mu = 1$ and $\mu \to \infty$, in dependence of the barrier E^* and the transfer distance ΔR. Two values of harmonic force constants k were chosen, and the corresponding two sets of bond dissociation energies D recalculated from E^* and ΔR. A short comment should be added: in order to get a broad survey of $\langle P \rangle^{qu}/\langle P \rangle^{cl}$ over E^* and ΔR, data with higher barriers (>1 eV) were included in Fig. 2. These data are reliable, both physically and computationally, with regard of the applied Franck–Condon approximation, but suffer in the kinetic respect from too low values of $\langle P \rangle$ at room temperature. We therefore attach no significance to absolute $\langle P \rangle$ data at this place. Quantal transitions with $\mu = 1$, referring to proton transfer between heavy atoms, are mostly restricted to low values of ΔR.

Table 2. Transition probabilities $\langle P \rangle$ for different potential shapes of initial and final states; fixed diabatic barrier height (diabatic crossing point) $E^* = 0.5$ eV

$k_a = 250\ \mathrm{N\,m^{-1}}$, $k_b = 125\ \mathrm{N\,m^{-1}}$; $E_M = 2$ eV; $V = 1$ eV; $\Delta E = 0$

T/K	ΔR/pm	D_a/eV	D_b/eV	μ/g mol^{-1}	$\lg\langle P_{a\to b}/\mathrm{s^{-1}}\rangle$
100	80	1.8	4.06	1	−13.1
				10	−24.9
				30	−30.1
				100	−32.6
				∞	−33.7
300	80	1.8	4.06	1	3.2
				10	0.1
				30	−0.24
				100	−0.37
				∞	−0.41
100	80	1.5	5.9	1	−13.1
				10	−25
				30	−30.2
				∞	−33.5
300	80	1.5	5.9	1	3.18
				10	0.14
				30	−0.17
				∞	−0.33
100	100	1.8	0.94	1	−14.6
				10	−26.4
				30	−28.2
				100	−28.9
				∞	−29.1
300	100	1.8	0.94	1	2.83
				10	1.37
				30	1.22
				∞	1.18

Figure 2 clearly shows how $\langle P \rangle^{qu}/\langle P \rangle^{cl}$ decreases with larger transfer distance ΔR, and increases with larger barrier height E^*. This general feature is also coarsely preserved with other realistic potential shapes, and with energy minima difference values $|\Delta E| > 0$. An analogous $\langle P \rangle^{qu}/\langle P \rangle^{cl}$ diagram over ΔR is shown in Fig. 3, for the experimentally relevant quantum range of medium-sized reduced mass, taken as $\mu = 30$. This diagram gives a quantitative survey of the error in $\langle P \rangle$ which is made when a real (quantal) system with effective mass of about 30 is approximated by the classical limit. As in Fig. 2, this limit is favoured for small barrier E^* and/or large transfer distance ΔR.

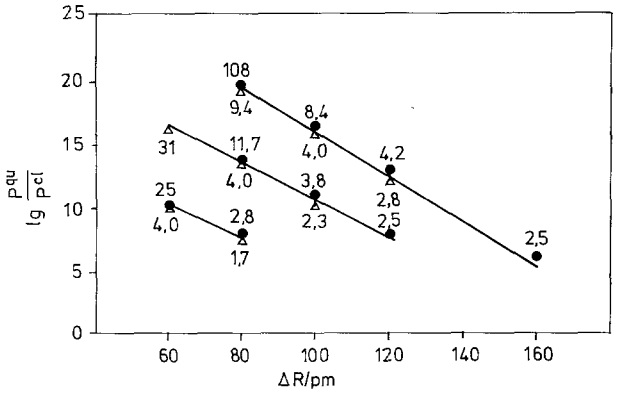

Fig. 2. Logarithmic transition probability quotient $\lg(\langle P\rangle^{qu}/\langle P\rangle^{cl})$, referring to reduced mass $\mu = 1$ (quantum regime) and $\mu \to \infty$ (classical regime), vs. transfer distance ΔR, for different diabatic barrier heights E^*: from bottom to top $E^* = 0.91$; 1.34; 1.75 eV. Equal but opposed initial and final potential shape: $k_a = k_b$, $D_a = D_b$, $\Delta E = 0$; $T = 300$ K. Label ● refers to $k_a = 400\ \mathrm{N\,m^{-1}}$, △ to $k_a = 600\ \mathrm{N\,m^{-1}}$. The D_a-values (in eV) corresponding to E^*, k_a and ΔR are given in the figure

3.3. Dependence of $\langle P\rangle$ in the classical limit at fixed barrier height, on the transfer distance ΔR: comparison of Franck–Condon models with the adiabatic activation picture

The familiar, classical activation picture predicts a rather insignificant dependence of rate constants on the adiabatic barrier breadth. A proof of this feature in the diabatic (or quasiadiabatic) Franck–Condon approach to chemical kinetics in condensed systems is so far lacking. The present application to strong anharmonic systems allows one to consider this question more closely.

Referring to Figs. 2 and 3, we add here the information that the corresponding $\lg\langle P\rangle^{cl}$ data in the classical limit and respectively at fixed E^*, differ only by 0.5 to 1 upon variation of ΔR. This statement holds for fixed electronic matrix

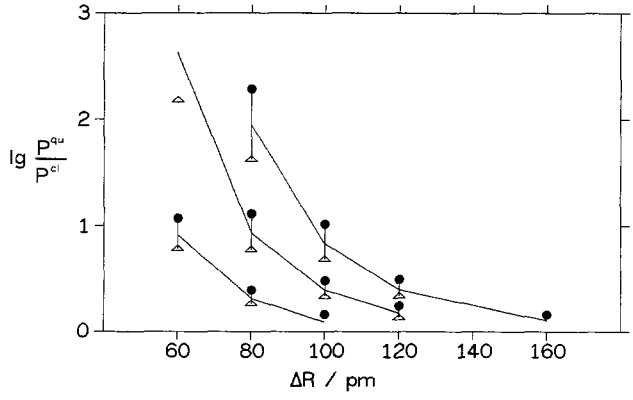

Fig. 3. Logarithmic transition probability quotient $\lg(\langle P\rangle^{qu}/\langle P\rangle^{cl})$, referring to reduced mass $\mu = 30$ (quantum regime) and $\mu \to \infty$ (classical regime), vs. transfer distance ΔR, for different diabatic barrier heights E^*. Parameters as Fig. 2

element V. One may expect however a decrease of V at larger ΔR (to be verified, in principle, by quantum-chemical calculations). Taking this trend into account, one expects a (moderate) decrease of $\lg\langle P\rangle^{cl}$ with increasing barrier breadth ΔR at fixed barrier height E^*. Returning to the adiabatic activation picture, this feature reflects the influence of excited adiabatic potential surfaces upon transition probabilities, which is neglected in the usual transition state theory. The Franck–Condon approach includes this influence via the electronic matrix element, which obeys the quasiadiabatic expression $V \simeq 0.5(E_2(R^*) - E_1(R^*))$, where E_1 and E_2 are adiabatic ground-state and excited-state potential surfaces taken at the diabatic crossing point R^*.

Minor improvement in these considerations may be possible if the activation barrier of the total system is fixed, rather than E^*. This will be addressed in Sect. 3.5.

3.4. Influence of transfer distance on tunneling in the quantum regime (small reduced mass)

The preceding discussion refers to the classical limit of transition probabilities. The quantum effect upon $\langle P\rangle$ is immediately given by the quotient $\langle P\rangle^{qu}/\langle P\rangle^{cl}$: examples of quantitative data for reduced mass $\mu = 1$ and $\mu = 30$ in Figs. 2 and 3 show the strong diminution of quantum effects with larger barrier breadth ΔR.

3.5. Relation of the barrier height E^* of the reactive subsystem to activation parameters of the total system

As addressed in the text to Fig. 1, the diabatic barrier E^* is a parameter of the reactive subsystem (including a minor medium effect on ΔE). A short comment is here given on the relation of E^* to a suitably defined total barrier (Arrhenius activation energy E_A). In the classical limit following Eq. (4), the activation energy E_A^{cl} may be chosen to be $e(R)$ in the exponent of Eq. (4), taken at the saddle coordinate R_s^{cl}, which is obtained from $de/dR = 0$ (the approximate validity of saddle-point integration of Eq. (4) taken for granted, as is the case in the following examples). Table 3 gives some data which show that E_A^{cl}

Table 3. Comparison of diabatic barrier E^* of the reactive subsystem and the corresponding crossing point coordinate R^*, with classical activation parameters E_A^{cl} and R_s^{cl} of the total system, obtained from Eq. (4): R_s^{cl} from $de/dR = 0$; $E_A^{cl} = e(R_s^{cl})$

$T = 300$ K; $\Delta E = 0$; $E_M = 2$ eV; $V = 1$ eV; $\Delta R = 120$ pm

k_a/N m^{-1}	k_b/N m^{-1}	D_a/eV	D_b/eV	E^*/eV	R^*/pm	E_A^{cl}/eV	R_s^{cl}/pm	$\frac{E_A^{cl} - E^*}{E_M}$
300	500	3	29	1.75	82	2.07	95	0.16
600	600	2.1	9.4	1.75	80	1.96	104	0.105
500	800	3	9.0	2.12	80	2.41	95	0.145
600	500	6	11.6	2.71	63	3.19	67	0.24

The last column shows the relative enhancement of E_A^{cl} over E^*, which turns out the smaller the larger the potential anharmonicities

exceeds E^* by a fraction of the medium reorganization energy E_M which depends on details of potential anharmonicities.

In general, the plot of $\lg\langle P\rangle$ over $1/T$ or β is nonlinear, especially in the quantum regime and at low temperature. The weakened temperature dependence of $\langle P\rangle$ at small reduced mass is well reflected in Tables 1 and 2. Calculational examples of T-dependent activation energies based on a special division of $\langle P\rangle$ into Arrhenius parameters are contained in [4, 5]. Theoretical problems of activation parameters have been discussed in [6].

3.6. Shift of $\langle P\rangle$ with medium reorganization energy: generalization to anharmonic subsystem coupled to harmonic medium

We mention here a slight generalization concerning the dependence of $\langle P\rangle$ on the medium reorganization energy E_M. Calculations prove that the shift $\partial \ln\langle P\rangle/\partial E_M \approx -1/4kT$ (with a minor decrease proportional to ΔE^2), which is valid in the classical, harmonic Marcus model, also holds when an anharmonic sub-system with arbitrary reduced mass (1 to ∞) is coupled to a harmonic medium.

The validity of harmonic solvent reorganization has been supported by recent simulation studies of outer-sphere electron transfer processes [7, 8]. The medium effect upon strong anharmonic chemical bond formation processes still requires closer consideration. Absolute estimates of $\langle P\rangle$ are, so far, mostly limited by the uncertainty in E_M.

This latter remark holds above all at low temperatures, as is illustrated by the two examples of Table 1. The upper example (corresponding to very flat potentials) includes an almost barrierless transition in the subsystem S. Nevertheless at $\mu = 1$ and 100 K, the transition probability, $\langle P\rangle$, is much smaller than in the lower example, despite a diabatic barrier E^* of more than 1 eV due to the small E_M assumed in the latter case.

3.7. Distribution of transition components and statistical lifetimes over initial-state vibration energy

We proceed now to a more detailed consideration of state-resolved properties of the overall chemical conversion process. Firstly we give in Fig. 4 an example of higher excited anharmonic initial and final vibration functions $|av\rangle$ and $|bw\rangle$ and their overlap product. The integral $\langle bw|av\rangle$ over the reaction coordinate constitutes the Franck–Condon factor which controls the individual transition component $P_{av\to bw}$ appearing in Eq. (1). The overwhelming influence of the outer wave function maxima upon the overlap product, typical for transfer processes over large ΔR, is apparent. In the classical limit these outer maxima turn to a δ-peak.

Examples of the transition component distribution $P_{av\to b}$ over the initial-state vibration energy E_{av} are given in Figs. 5 and 6, for different reduced mass. $P_{av\to b}$, following Eq. (2), gives the transition probability from one thermally weighted initial state av into any final states b. The distribution $P_{av\to b}(E_{av})$ degenerates in the classical limit into a continuous distribution $P(E_a)^{cl}$ following Eq. (7).

Figures 5 and 6 correspond to the first two examples given in Table 2. The upper part of Fig. 5 shows the discrete distribution $P_{av\to b}(E_{av})$ in the quantum regime for reduced mass $\mu = 1$, 10, 30, and the continuous distribution $P(E_a)^{cl}$ at

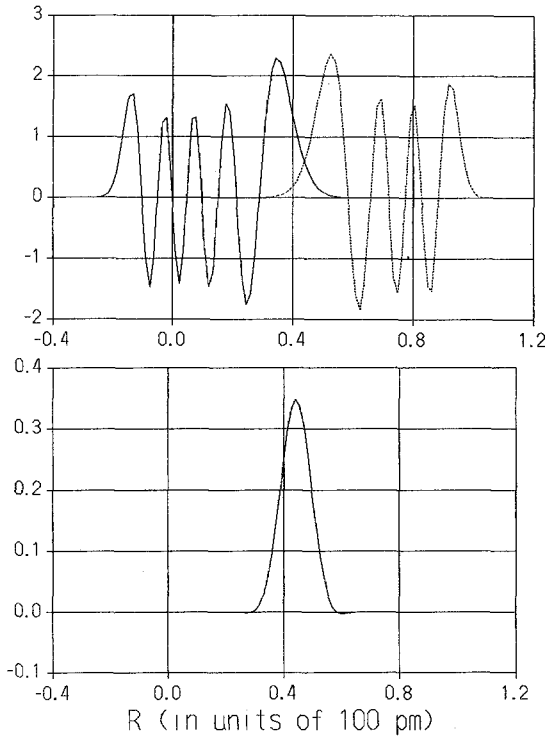

Fig. 4. Examples of higher excited vibration functions ϕ_{av} and ϕ_{bw} in anharmonic diabatic initial and final potentials (*top*) and their overlap product $\phi_{av} \cdot \phi_{bw}$ (*bottom*), vs. reaction coordinate R. Quantum states $v = 8$, $w = 6$. Parameters: $k_a = k_b = 600\ \mathrm{N\,m^{-1}}$, $D_a = D_b = 1.68\ \mathrm{eV}$, $\Delta R = 80\ \mathrm{pm}$, $\mu = 10\ \mathrm{g\,mol^{-1}}$

$\mu \to \infty$, all taken at 300 K. One recognizes that the distribution maxima are shifted to lower P-values and to higher energies E_a when μ increases from 1 to ∞. Figure 6 shows, for the same system, the distribution pattern at 100 K. At low temperature, the distribution maxima typically lie at lower energies than at 300 K, and at extreme P-values.

In the lower part of Fig. 5, the distribution of statistical lifetimes τ_{av} of initial states in a canonical ensemble, up to reactive transition into a final state is shown. The reciprocal lifetime $1/\tau_{av}$, following Eq. (3), represents simply the transition component $P_{av \to b}$, divided by the Boltzmann factor of state av, irrespective of the frequency of thermal transitions within the initial series of states. The short-time, or high-energy branch of the lifetime distribution $\tau_{av}(E_{av})$ gives a rough indication of the limitations of the canonical approximation (Eqs. (1) or (4)) due to onset of interference with time scales of dynamical equilibration processes. This point will be considered further in Sect. 3.8.

Division of $P_{av \to b}$ into the individual transitions into final states bw yields, for given av, the distribution of $P_{av \to bw}$ over final states bw. Table 4 shows for the maximal transition component ($av = 5$) at $\mu = 10$ of Fig. 5, the distribution of the relative transition components ($P_{a5 \to bw}/P_{a5 \to b}$) and the corresponding Franck–Condon overlap $\langle bw | a5 \rangle$ which increases typically with higher final-state functions bw.

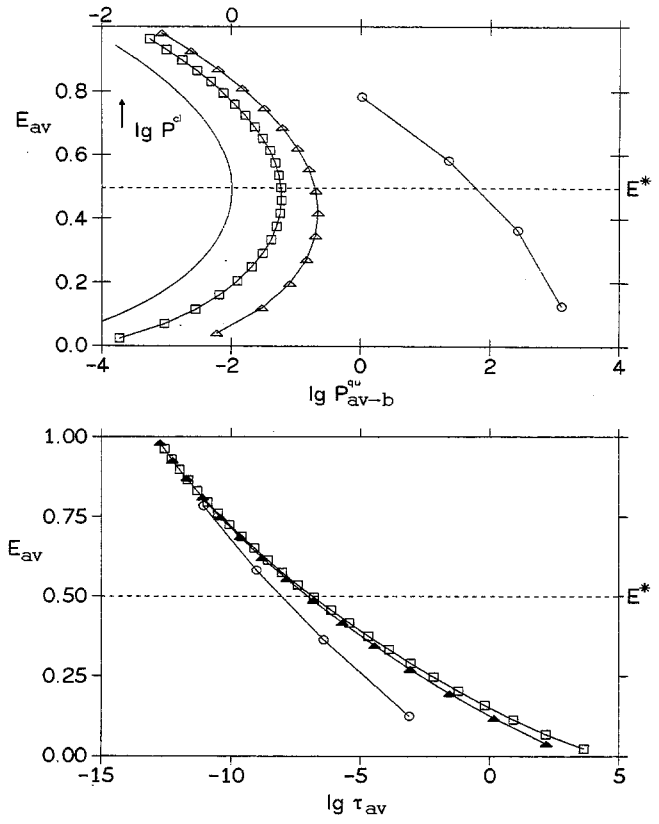

Fig. 5. Quantal and classical distribution of transition components (*top*) and of statistical lifetimes (*bottom*), vs. initial-state vibration energy. Reduced mass from right to left: $\mu = 1$; 10; 30 (quantum regime); ∞ (classical regime) $P^{qu}_{av\to b}/s^{-1}$ from Eq. (2), $P(E_a)^{cl}/s^{-1}\,eV^{-1}$ from Eq. (7). τ_{av}/s from Eq. (3). Potential parameters: $k_a = 250\ N\,m^{-1}$, $D_a = 1.8$ eV, $k_b = 125\ N\,m^{-1}$, $D_b = 4.06$ eV, $\Delta R = 80$ pm, $\Delta E = 0$, $E_M = 2$ eV, $E^* = 0.5$ eV, temperature 300 K

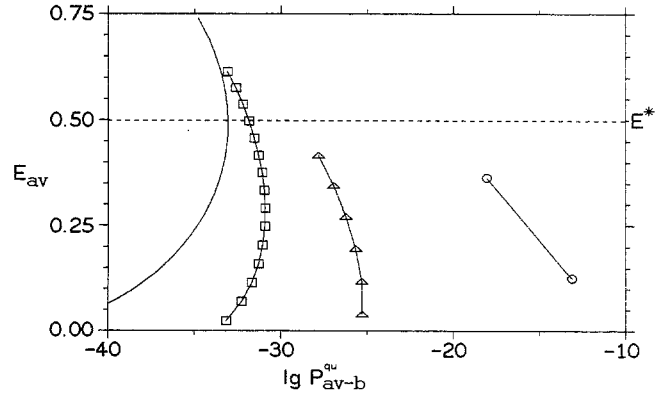

Fig. 6. Quantal and classical distribution of transition components vs. initial-state vibration energy. Conditions as Fig. 5, but temperature 100 K

Table 4. Franck–Condon overlap $\langle bw|av\rangle$ of the maximal transition component shown in Fig. 5 for $\mu = 10$, into those final states which contribute 99% to $P_{av\to b}$

$\Delta R = 80$ pm, $k_a = 250\ \mathrm{N\,m^{-1}}$, $k_b = 125\ \mathrm{N\,m^{-1}}$, $D_a = 1.8$ eV, $D_b = 4.06$ eV, $E_M = 2$ eV, $\Delta E = 0$

av (max)	bw	$\frac{P_{a5\to bw}}{P_{a5\to b}} \cdot 1000$	$\langle bw\|a5\rangle$
5	3	7	0.001
	4	22	0.003
	5	57	0.008
	6	109	0.02
	7	164	0.04
	8	196	0.08
	9	184	0.1
	10	135	0.2
	11	77	0.25
	12	32	0.3
	13	9	0.3

3.8. Discussion of dynamical equilibration effects on transition component distribution and on total transition probability

Finally in this paper, we ask briefly for the short-time limits of canonical transition probabilities following Eq. (1) or (4), coarsely attained in the time scales of equilibration dynamics of the reactive subsystem as well as of the medium, or the different parts of the medium (in cases of interfacial processes). Our present knowledge of these processes is incomplete. We therefore restrict ourselves to a preliminary discussion focussing on not too fast reactions.

Three kinds of dynamical processes are relevant in the present context: (I) the relaxation, following the preparation of the initial state of the reactive subsystem, into a canonical distribution; (II) relaxation of the solvent part of the medium; and (III) relaxation of the lattice part, in interfacial processes.

Processes of type (I) depend on the phonon interaction dynamics between the subsystems S and M, as is also the case in other energy exchange processes, e.g. thermal accommodation. According to classical arguments, such processes are very fast ($< 10^{-13}$ s); related quantum effects are, as yet, largely unexplored.

Processes of type (II) have received greater attention in recent years (cf. [9–12] and references therein). According to these treatments, the solvent reorganization dynamics is controlled by the spectrum of longitudinal dielectric relaxation [9, 10]. Information is experimentally accessible in fast optical or electron transfer processes in solvents with higher viscosity. Slow solvent dynamics leads to diminution of $\langle P\rangle$ relative to the canonical, or sudden, approximation. This diminution can, however, be suppressed by fast dielectric relaxation, small electronic matrix element V (favoured in outer-sphere electron transfer over larger distance, not to be confused with heavy-particle transfer), or, following an argument in [11], by small Franck–Condon overlap. The latter factor is relevant in chemical conversion processes with a broad transition component distribution (cf. Fig. 5 and Table 4). One generally concludes that, if at all, the upper

branch of the $P_{av\to b}(E_{av})$ distribution can become dynamically affected. For chemical conversion in aqueous medium at room temperature, we estimate a possible dynamical effect amounting to a factor <2 in $\langle P\rangle$, which is far below the present uncertainty in static medium reorganization effects.

Lattice reorganization (process (III) addressed above), in addition to solvent reorganization, has been considered in [6, 13], in the sudden approximation. Lattice equilibration after a perturbation should again be controlled classically. Special quantum (e.g. plasmon) excitations are not known to be relevant in the energy range under consideration.

4. Summary

In this paper, the long-standing problem of the relation of the quantum to the classical regime and of the conditions of the classical approximation of nuclear motion in elementary chemical processes has been considered, with view on two actual but so far yet unexplored aspects: firstly, we proceed from Franck–Condon transitions in diabatic potentials, which are particularly suited for treating reactive processes in condensed systems, including chemical bond formation and partial charge transfer; secondly we take into account heavy-particle transfer in strong anharmonic potentials allowing for transfer over larger distances.

A synopsis of numerical data is given which illustrate the effects of finite to infinite reduced mass of a 1D reactive mode (quantum to classical regime), upon total transition probabilities and transition component distributions, in dependence of the diabatic barrier height of the reactive subsystem and the transfer distance (barrier breadth). The dependence of transition probability on the medium reorganization energy, and the limits of the canonical, or sudden, approximation of Franck–Condon transitions due to finite equilibration times of the reactive mode and the medium were also briefly considered. The present calculations are confined to 1D potentials of Morse type. Several quantal and classical problems with multidimensional, non-separable potentials (partly addressed in [14]) are related to the present theme.

Appendix: Calculational annotations

We add some calculational details to Sect. 2. The Franck–Condon overlap $\langle bw|av\rangle$ which enters into the transition elements $T^S_{bw,av}$ of Eq. (1) has been calculated using Morse functions

$$\phi_v(z) = N_v \cdot \exp(-z/2) \cdot z^{\alpha/2} \cdot L_{v+\alpha}(z) \tag{A1}$$

with

$$\begin{aligned} N_v &= \{[a\alpha v!]/\Gamma(\alpha+v+1)\}^{1/2}, \\ z &= 2\beta \cdot \exp(-a(R-R_0)), \quad \alpha = 2\beta - 2v - 1, \quad \beta = k/a^2\hbar\omega, \\ L_{v+\alpha}(z) &= \sum_{l=0}^{v} (-1)^{v-l} \cdot (l!(v-l)!)^{-1} \cdot (\alpha+v)_l \cdot z^{v-l}, \\ (\alpha+v)_l &= (\alpha+v)(\alpha+v-1)(\alpha+v-2)\cdots(\alpha+v-l+1), \end{aligned} \tag{A2}$$

where v is the vibration quantum number, k the harmonic force constant, μ the reduced mass, $\omega = (k/\mu)^{1/2}$, a the anharmonicity constant, and L are Laguerre polynomials. Analytical expressions for Morse overlap are available only for special cases; on the other hand, the numerical calculation of $\phi_v(z)$ from (A1, A2) fails for higher quantum numbers $v \gtrsim 4$, because of alternating signs of an increasing number of terms in the Laguerre polynomials. An expedient solution is the recursive calculation of higher Morse functions [15] from

$$\begin{aligned} \exp(-a(R-R_0)) \cdot \phi_v &= A_v \phi_v + B_v \phi_{v-1} + B_{v+1} \phi_{v+1}, \\ A_v &= [2\beta(v+1/2) - v(v+1)]/[(\beta - v)(\omega - v - 1)], \\ B_v &= \beta/2(\beta - v) \cdot \{[v(2\beta - v)]/[(\beta - v - 1/2)(\beta - v + 1/2)]\}^{1/2}, \end{aligned} \tag{A3}$$

as proposed in [16]. This immediately allows the recursive calculation of Franck–Condon overlap [3] up to high quantum numbers, v, w, with negligible numerical error depending on the number of integration intervals.

The quantum to classical relation of conversion probabilities following Eqs. (1) and (4) can be straightforwardly extended to separable many-dimensional potentials, as will be outlined in a broader context in [17].

References

1. Engler C, Rabe E, Schultz H, Lorenz W (1989) Theor Chim Acta 75:67
2. Lorenz W, Engler C (1984) Phys Stat Sol B122:745
3. Engler C (1984) Z Phys Chem 265:1193
4. Engler C, Lorenz W (1984) J Electroanal Chem Interfacial Electrochem 171:123
5. Engler C, Wiegratz S (1986) Z Phys Chem 267:365
6. Lorenz W, Engler C (1986) J Electroanal Chem Interfacial Electrochem 204:13
7. Hwang JK, Warshel A (1987) J Am Chem Soc 109:715
8. Kuharski RA, Bader JS, Chandler D, Sprik M, Klein ML, Impey RW (1988) J Chem Phys 89:3248
9. Sumi H, Marcus RA (1986) J Chem Phys 84:4272
10. Wolynes PG (1987) J Chem Phys 86:5133
11. Jortner J, Bixon M (1988) J Chem Phys 88:167
12. Sparpaglione M, Mukamel S (1988) J Chem Phys 88:3263
13. Engler C, Rabe E (1986) Phys Stat Sol B138:477
14. Lorenz W, Heitzsch O (1989) Theor Chim Acta 76:137
15. Magnus W, Oberhettinger F, Soni RP (1966) Formulas and theorems for the special functions of mathematical physics, 3rd edn. Springer, Berlin Heidelberg New York, p 241
16. Tran LB, Huffaker JN (1983) J Math Phys 24:397
17. Engler C, Lorenz W; in preparation